Angle and Polarization Insensitive Mid-Infrared Optical Filters Using Dense 2D Array of Nanophotonic Cavity Resonators

Matthew Klein, Shivashankar R. Vangala, Joshua R. Hendrickson, and Ivan Avrutsky

***Abstract*—We report on the design and experimental verification of angle and polarization insensitive mid-infrared filters based on dense arrays of dielectric resonators embedded into a metallic film. We experimentally show filters with 60% peak transmission for angles from 0 to 60 degrees for perpendicular polarization states. We also study the surface plasmonic mode excited due to the periodicity of the micro-resonators in the array. Simulations support the experimental results for both the primary resonance and the plasmonic mode. Integrating these filters with IR detectors offers multispectral imaging and improved search and track capability.**

***Index Terms*—Infrared photonics, infrared filters, resonant transmission.**

I. Introduction

ANGLE-INDEPENDENT narrow-band spectral filters based on a dense array of micro-resonators [1], [2], [3], [4] enable further improvement of multi-spectral mid-infrared filtering (MIRF) systems [5] working with wide-angle imaging optics. The micro-resonators in such a device are cavities, often, but not necessarily, in the form of cylindrical holes, implemented in a metallic film held by a transparent substrate. The cavity resonances are non-plasmonic in nature. Filling the cavities with a high-index dielectric helps reduce the lateral size of the micro-resonators down to dimensions that are at the sub-wavelength scale in the low-index substrate and cover media. Each micro-resonator has a broad acceptance angle, and it also emits light into a broad range of angles, which eventually enables filter's characteristics that are largely angle-independent.

A Broader perspective of the technical solutions for optical transmission filters with various levels of angle-(in)dependent operation includes all-dielectric [6] or metal-dielectric [7], [8] multilayers and plasmonic structures [9], [10], [11], [12], [13] employing propagating or localized modes. Narrowband transmission notch-filters based on waveguide grating resonances [14], [15], [16], [17], [18] as a rule are strongly angle-dependent, while structured period gratings may help in achieving angle-independence within some limited range of angles of incidence [19], [20]. Depending on the application, each of these technical solutions can be tailored to deliver excellent performance. With mid-infrared multi-spectral imaging in mind, this study is focused on filters based on dense arrays of micro-resonators. By tuning the height, diameter, and period of the micro-resonator array, it is possible the change the spectral response of the filter, which will in turn allow for a filters of varied spectral responses to be fabricated onto a single chip. This will lead to designer, pixel scale filters that can be integrated with existing detector architectures.

When micro-resonators in a dense array are excited by a plane wave, the oscillations in individual micro-resonators are synchronized due to the common excitation, and the waves emitted by the micro-resonators collectively form a transmitted plane wave. Aside from the common excitation by an incident wave, the micro-resonators should operate independently from one another in order to make sure the transmission spectra are angle-independent.

A weak coupling between the micro-resonators that arises from placing the cavities too close together leads to formation of an excitation that propagates along the surface of the film, hopping from one cavity to the next and so forth. Phase matching between the incident wave and such a surface excitation in a periodical array of micro-resonators will then lead to angle-dependent resonances similarly to grating-assisted excitation of guided modes or surface plasmon-polaritons. In the system under study, we place the micro-resonators sparsely enough to avoid coupling between them, but densely enough to provide strong resonant transmission. Periodicity as such is not critical for the operation of this filter.

The resonant wavelength of such transmission filter can be estimated based on the following considerations. In the cylindrical dielectric cavity, the light wave propagates back and forth as a traveling mode of a cylindrical metallic pipe waveguide, distinctly different from a metal-insulator-metal or insulator-metal-insulator resonance to which it bears a close resemblance. The TE_{11} mode in the metallic pipe waveguide has the longest

Manuscript received 15 December 2023; revised 29 February 2024; accepted 20 March 2024. Date of publication 25 March 2024; date of current version 2 April 2024. This work was supported by the Air Force Office of Scientific Research under Grant FA9550-23RYCOR001 and Grant FA9550-20RYCOR059 (Program Manager Dr. Gernot Pomrenke). Ivan Avrutsky was supported by AFOSR SFFP program. *(Corresponding author: Matthew Klein.)*

Matthew Klein is with KBR, Beavercreek, OH 45431 USA, and also with Air Force Research Laboratory, Sensors Directorate, Wright-Patterson AFB, OH 45433 USA (e-mail: Matthew.Klein.10.ctr@us.af.mil).

Shivashankar R. Vangala and Joshua R. Hendrickson are with Air Force Research Laboratory, Sensors Directorate, Wright-Patterson AFB, OH 45433 USA.

Ivan Avrutsky is with the Department of Electrical and Computer Engineering, Wayne State University, Detroit, MI 48202 USA.

Digital Object Identifier 10.1109/JPHOT.2024.3381548

cutoff wavelength λ_c that can be found from the following equation

$$\frac{2\pi}{\lambda_c} nR \approx 1.8412. \tag{1}$$

Here, the metal is assumed to be ideal, the radius of the cylindrical pipe waveguide is R, and the cavity is filled with a dielectric with refractive index n. The particular value of the constant at the right side of (1) equals to the first root of the derivative of the first-order Bessel function $J_1'(x)$. In the case of realistic metals, the electromagnetic field of the guided mode penetrates beyond the surface of the metal, which effectively makes the radius somewhat larger.

Although the TE_{11} mode of the cylindrical metallic pipe waveguide is not linearly polarized, it does have a preferential direction for the electric field vector. Similar to the case of plane waves propagating in free space, the cylindrical geometry supports two degenerate TE_{11} modes with the preferential polarization directions orthogonal to each other. The degeneration of the TE_{11} modes allows for choosing one of the preferential polarization direction at will, for instance to match the polarization of the incident wave. This enables coupling between the linearly polarized incident plane wave and the cavity mode and makes the coupling largely polarization independent.

The cutoff wavelength λ_c defines the dispersion of the modal index:

$$n^* = n\sqrt{1 - \left(\frac{\lambda}{\lambda_c}\right)^2} \tag{2}$$

Interestingly, the modal index is lower than the refractive index of the dielectric in the cavity. If the cavity is filled with air, the modal index becomes smaller than unity, and the phase velocity in the pipe waveguide exceeds the speed of light in free space.

To find the m-th order resonant wavelength ($m = 1$ for the fundamental mode), the round-trip phase accumulation in the resonator is set to $2\pi m$:

$$2L \cdot \frac{2\pi}{\lambda} n^* + \psi_c + \psi_s = 2\pi m. \tag{3}$$

Here, L is the height of the dielectric cylinder, ψ_c and ψ_s are the values of phase that the guided mode obtains at reflections from the interfaces with the cover and substrate respectively. The resonant wavelength then is

$$\lambda = 2Ln\sqrt{1 - \left(\frac{\lambda}{\lambda_c}\right)^2}\left(m - \frac{1}{2\pi}(\psi_c + \psi_s)\right)^{-1} \tag{4}$$

The value of the fundamental resonant wavelength thus is set mainly by the refractive index and the height of the resonator: $\lambda \approx 2Ln$, exactly at the wavelength of maximal transmission in the case of normal incidence at a flat high-index film with thickness L and refractive index n. Then, the modal index n^*, being lower than the index n of the dielectric pushes the resonant wavelength towards smaller values. The nonzero phases of reflections ψ_c and ψ_s at the substrate and cover media contribute towards making the resonant wavelength longer. The latter effect apparently prevails. In a sense, the nonzero reflection phases make the resonator effectively somewhat longer. Depending on the configuration, the resonant wavelength in the filters under study may be up to 50% larger than the product $2Ln$. In any case, the height of the resonator L is the major parameter to be adjusted when it comes to the necessity of adjusting the resonant wavelength.

The spectral width of the fundamental transmission resonance is defined by the losses in the resonator, both due to absorption in the metal and due to imperfect reflection at the interfaces with the substrate and cover. Absorption in the metal walls leads to a complex value of the modal index n^*. The round-trip attenuation factor associated with the absorption is given by $exp(-\frac{4\pi}{\lambda} Im(n^*) \cdot 2L)$. Further contribution to the round-trip attenuation is due to non-unity reflection coefficients R_s and R_c describing the power reflections at the substrate and cover. The quality factor of the fundamental resonance then becomes

$$Q = 2\pi \cdot \left(1 - R_s R_c \exp\left(-\frac{4\pi}{\lambda} Im\left(n^*\right) \cdot 2L\right)\right)^{-1} \tag{5}$$

Finally, the spectral width of the transmission line is estimated at

$$\Delta\lambda = \lambda/Q \tag{6}$$

In case of lossless metal, higher reflection coefficients R_s and R_c, and thus higher Q-factor, are expected for resonators with smaller radius – as long as the operating wavelength remains shorter than the cutoff wavelength. With real metals however, reduced radius of the cavity also leads to increased absorption in the metal, pushing the Q-factor down.

To increase the reflection coefficients R_s and R_c, one can also explore a more sophisticated geometry of the micro-resonators, such as adding thin metallic films with small apertures at the interfaces with the substrate and cover. This modification of geometry will also change the phases of reflection ψ_c and ψ_s with corresponding change of the resonant wavelength. From the manufacturability perspective, it is preferable to work with the simplest geometry.

The transmission resonance associated with excitation of the micro-resonators in the system arranged in a square lattice is expected to be both angle- and polarization-insensitive. However, if there are other spectral features that are angle-dependent, they can experience a spectral shift with incident angle deviating farther from the normal, and eventually overlap to some degree with the transmission resonance under study. The most notable examples are Rayleigh resonances linked to diffracted waves transitioning between the propagating and evanescent regimes and excitation of surface plasmon-polariton modes which for first-order diffraction follow the condition

$$\left(\frac{2\pi}{\lambda}\right) * \sin(\theta) \pm \left(\frac{2\pi}{\Lambda}\right) = \pm\left(\frac{2\pi}{\lambda}\right) n_{eff} \tag{7}$$

At normal incidence these spectral features are located at $\lambda \approx \Lambda n_c$ and $\lambda \approx \Lambda n_s$ for the waves in cover and substrate respectively. They move with angle of incidence θ according to

$$\lambda_{c,s} \approx \Lambda\left(n_{c,s} \pm \sin\theta\right) \tag{8}$$

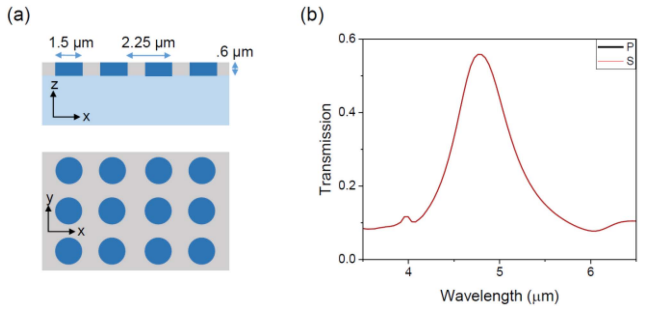

Fig. 1. (a) Cross-section (upper) and top-view (lower) of the MIRF device where the sapphire substrate is light blue, germanium resonators are dark blue, and silver film is grey. The resonators are 1.5 μm in diameter, 0.6 μm tall, with a period of 2.25 μm in both x and y directions (denoted by axis). (b) Simulated transmission spectra at normal incidence for P-polarized plane waves shown in black and S-polarized plane waves shown in red.

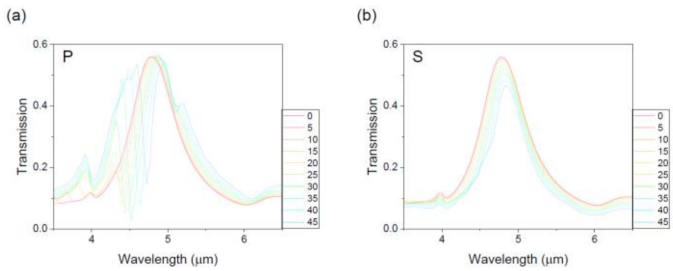

Fig. 2. (a) Transmission spectra for P-polarized plane waves for different angles of incidence. (b) Transmission spectra for S-polarized plane waves at different angles of incidence.

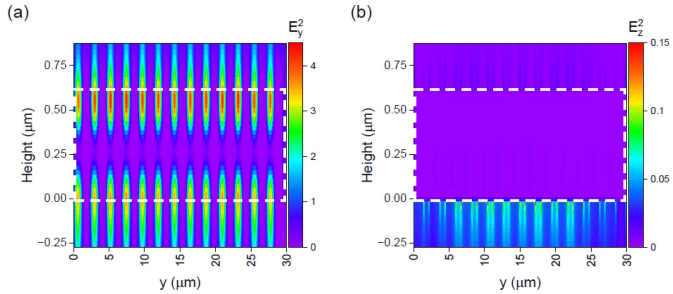

Fig. 3. (a) Electric field profile of the cavity mode at the center of the resonance (4.6 μm) for y-polarized excitation. (b) Electric field profile of the plasmonic mode at the plasmonic resonance (3.8 μm) for y-polarized excitation. The region of the designed array is denoted by white dashed lines.

By reducing the period Λ of the structure one can prevent these angle-dependent features from moving into the spectral range of interest.

The above considerations show the internal connections between the physical parameters that define the resonant transmission in the system under study. In this study we report experimentally verified improved, characteristics of angle-independent narrow-band mid-IR spectral filters, based on a dense array of micro-resonators.

II. 2D Array of Nanophotonic Cavity Resonators

A. Modeling

Our structure consists of an array of cylindrical germanium(navy) micro-resonators embedded into a silver film(grey) on a sapphire substrate (light blue), as shown in Fig. 1(a). We choose dimensions of 1.5 μm diameter, 2.25 μm period, and 0.6 μm height to place the fundamental resonance of the resonator around 4.75 μm, in order to avoid water absorption bands in the mid-IR. These dimensions also place the substrate plasmonic resonance at 3.75 μm at normal incidence which also allows for it to be studied at the same time as the primary resonance. Resonant excitation of plasmonic modes at the interface with air happens at a much shorter wavelength that is close to the period of the structure – the spectral range outside of the scope of interest in this study. This structure is then simulated using a plane wave source in Lumerical's FDTD solver. The simulated transmission spectra of this structure at normal incidence is shown in Fig. 1(b). where there is a strong primary resonance at 4.75 μm for both P (x-direction) and S (y-direction) polarizations. A weak plasmonic resonance also shows up around 3.75 μm as predicted. To show the angle-insensitivity of the filter, the simulation was then run at various angles of incidence. The simulated transmission spectra for P and S-polarizations at different angles of incidence are shown in Fig. 2(a), (b). Here, the primary resonance is maintained at 4.5 μm for angles up to 45 degrees angle of incidence for both P and S polarizations. The primary resonance only shows a marginal reduction to its amplitude while the plasmonic resonance in the P-polarized spectrum traverses across the primary resonance at increasing angles while there is very little change in the S-polarized plasmonic resonance. This is due to P-polarization being in the plane of rotation, while the S-polarization is perpendicular, which implies that significant changes should only be shown in the P-polarized spectra.

To confirm that the spectral response is coming from the expected sources, the intensity profile for y-polarized incident light is shown for E_y^2 on resonance (4.6 μm) in Fig. 3(a) and E_z^2 is shown near the plasmonic resonance (3.8 μm) in Fig. 3(b). Here, the cavity mode is confined to the resonator pillars within the designed array (white dashed) and the plasmonic mode has an out-of-plane component at the bottom surface of the array away from the dielectric cavities consistent with a surface plasmon resonance.

We further confirm (4)'s primary dependence on the thickness and not diameter or periodicity by scanning each feature while holding the other two constant (height 0.6 μm, diameter 1.5 μm, and period 2.25 μm). Fig. 4(a) shows the transmission response of the filter for varying resonator height where there is a primarily linear relationship between the resonant wavelength and the height of the resonators as expected with the plasmonic resonance being constant at $\sim$3.9 μm. There is a significant change in the spectral response of the filter after a diameter of 2.25 μm, which is due to the resonators overlapping and no longer being discrete. Tuning the diameter, as shown in Fig. 4(b) slightly shifts the location of the cavity resonance while maintaining a constant plasmonic resonance. Instead, the primary responsibility of the diameter is to tune the linewidth and amplitude of the resonance by accepting more or less light. The primary effect of the period

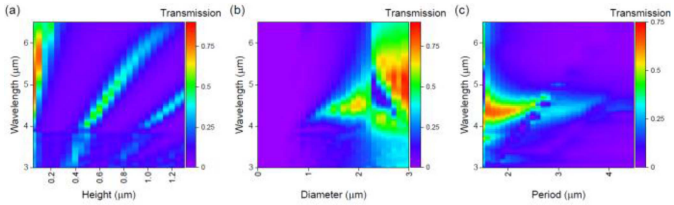

Fig. 4. (a) Colormap of the transmission response as a function of resonator height with constant diameter (1.5 μm) and period (2.25 μm). (b) Colormap of the transmission response as a function of resonator diameter with constant height (0.6 μm) and period (2.25 μm). Colormap of transmission response as a function on resonator period with constant height (0.6 μm) and diameter (1.5 μm).

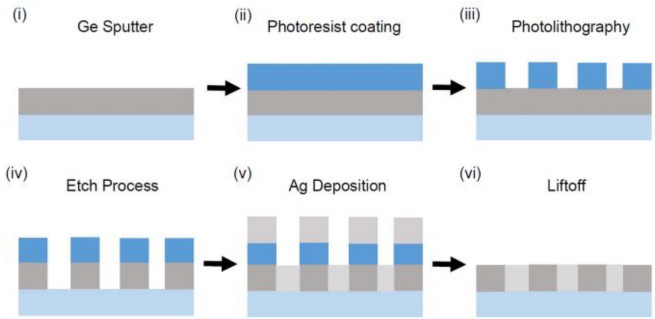

Fig. 5. MIRF fabrication process with the sapphire substrate in light blue, photoresist in dark blue, germanium in dark grey, and silver in light grey. (i) Sputtering a Ge film onto a clean sapphire substrate. (ii) Spin coating of the photoresist. (iii) Photolithography for patterning the etch mask. (iv) Fluorine based RIE or chlorine based ICP for patterning the Ge resonators. (v) Electron-beam evaporation of the silver film surrounding the resonators. (vi) Liftoff of the photoresist and the extra deposited silver.

is a reduction in the amplitude of the cavity resonance due to a reduced density of the resonators. The plasmonic mode is shown to linearly progress across the spectrum with increasing period as predicted by (8).

B. Fabrication

In order to measure the spectral response of the resonant filters, a multistep fabrication process is followed as shown in Fig. 5. Clean c-plane sapphire wafers (University Wafer) are RF sputtered with 600 nm of Germanium at 10 mTorr. The samples are then dehydration baked at 110 °C for several minutes and allowed to cool before being spin coated with ~1.7 μm of either SPR 955 or nLOF 2020 photoresists. The resist is then cured at 110 °C for 60 s. The samples are then patterned using i-line photolithography and baked again at 110 °C for 60 s. The samples are developed in 300 MIF for 60 s at 50 rpm before being rinsed with DI water and blown dry with N_2. A 4 min. O_2 plasma ashing is used to descum any photoresist residue left over from the development process. The samples are then etched using either a fluorinated reactive ion etch (RIE) recipe or a chlorinated inductively coupled plasma (ICP) recipe. The ICP recipe is favored due to the lack of the passivation layer left by the RIE which cannot be easily removed without damaging the Ge resonators. 600 nm of silver is then electron-beam deposited onto the samples at 5 A/s. The liftoff process was performed

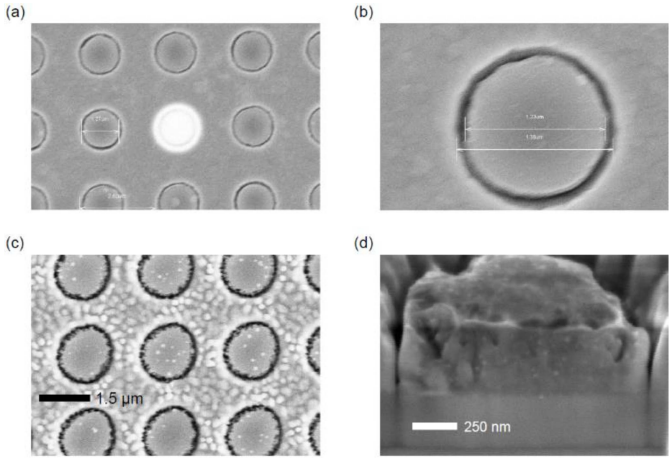

Fig. 6. (a) 13k magnification SEM image of the RIE etched MIRF device. (b) 50k magnification of one of the resonators shown in (a). (c) 18k magnification SEM Image of the ICP etched MIRF device. (d) FIB cut cross-section of the ICP etched device.

by sonicating the samples in either acetone (SPR 955) or NI555 (nLOF) until the resist was completely removed. The samples were then rinsed off in DI water and blown dry with N_2.The filters were then imaged using a scanning electron microscope (SEM) operated with a 10 kV acceleration voltage. A 13k magnification SEM image of an RIE sample is shown in Fig. 6(a). where the germanium resonators can be differentiated from the silver via contrast. The bright spot in the center of the image is from the resonators being removed from the sample. A 50k magnification SEM was then performed on a single resonator shown in Fig. 6(b). to best determine the dimensions of the structure. On this particular sample, the diameter was measured to be 1.23 μm with a period of 2.25 μm. There is also a noticeable air gap between the resonators and the silver of 0.14 μm.

Similar imaging was performed for an ICP etched sample as shown in Fig. 6(c). Here, the surface of the silver is noticeably rougher than in the RIE sample, which is due to the chlorinated chemistry etching into the sapphire substrate; whereas, the fluorinated chemistry does not. In this sample there is also a smaller air gap between the germanium and the silver, due to the lack of a passivation layer forming during the etching process. A focused ion beam (FIB) was then used to obtain a cross-section of the device. The cross section obtained from the ICP sample is shown in Fig. 6(d). where there is only an air gap near the top of the structure and not near the bottom.

III. Experimental Verification

In order to measure the transmission response of our filters, we use an FTIR based ellipsometer in transmission mode. The transmission spectra for the RIE sample is shown in Fig. 7(a), (b) for P and S polarizations respectively. At angles below ~6 degrees there is a single primary resonance at 4.75 μm for both the P and S polarizations with peak transmission reaching above 70%. As the angle increases, the amplitude and shifts in the substrate plasmonic resonance, centered around 4.1 μm at 0 degrees, becomes more prominent as it begins to overlap

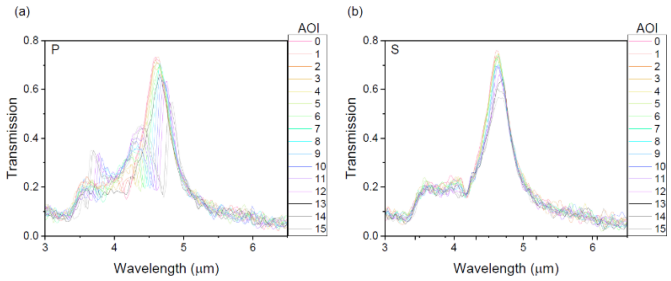

Fig. 7. P-polarized (a) and S-polarized (b) transmission spectra of a RIE fabricated device for angles of incidence up to 15 degrees.

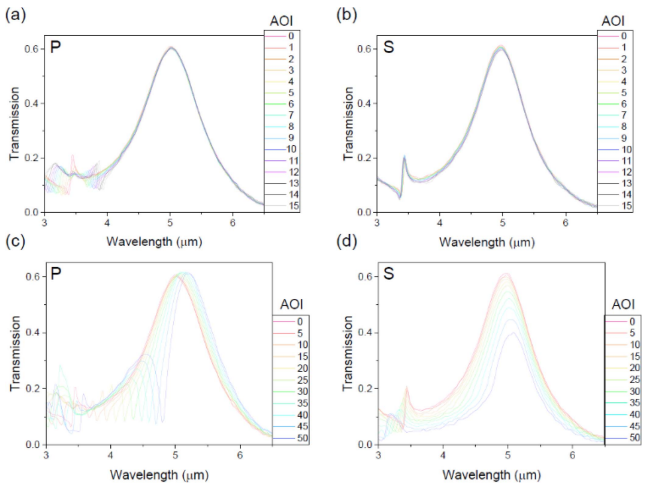

Fig. 8. P-polarized (a) and S-polarized (b) transmission spectra for an ICP fabricated device for angles of incidence up to 15 degrees. P-polarized (c) and S-polarized (d) transmission spectra for an ICP fabricated device for angles of incidence up to 50 degrees.

with the primary resonator resonance. This is due to the large air gaps in the RIE samples allowing for the light to more readily couple into the plasmonic mode by using the airgap to bypass to resonator. As shown in Figs. 7(a) and 8(a), there is a substrate plasmonic resonance that occurs at 4.1 μm and 3.75 μm at 0 degrees angle of incidence, respectively (with the difference in resonant location being due to a difference in the period of the structures). In both cases, as the angle of incidence increases the substrate plasmonic resonance has a blue shifting and red shifting component where the red shifting component is generally more pronounced due to its overlap with the primary resonance of the filter. This follows along from our theoretical prediction in (8) where the $\pm \sin\theta$ term should lead to a splitting of the substrate plasmonic resonance that increases with increasing angle of incidence.

In the ICP samples, the primary resonance is at $\sim$5 μm with a 60% transmission and the plasmonic resonance with the sapphire substrate at 3.5 μm for normal incidence. The transmission amplitude is reduced compared to RIE samples due to having a rougher surface of the germanium causing larger insertion losses into the resonator mode. At angles of incidence below 15 degrees shown in Fig. 6(a), (b), there is very little change in the P-polarized spectra and no change in the S-polarized spectra. We attribute this to a smaller air gap

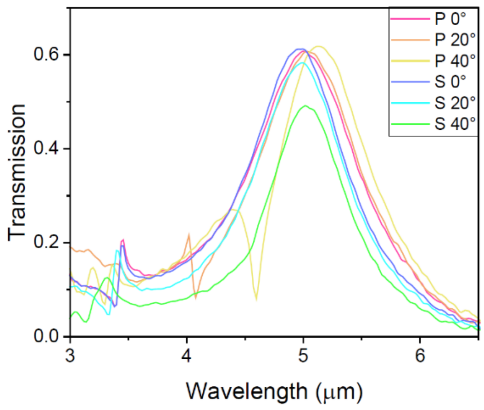

Fig. 9. Transmission spectra for both P and S -polarized light incident at 0, 20, and 40 degrees angle of incidence.

between the resonators and the silver film. The experiment is then further extended to investigate if there is any change in the spectra at even larger angles of incidence. The spectra of P and S transmission spectra up to 50 degrees angle of incidence are shown in Fig. 8(a), (b). In the transmission spectra of the P-polarization, a plasmonic absorption resonance appears which has both red and blue shifting components as predicted by (7). This effect is noticeably weaker in the ICP sample, compared to the RIE sample, due to having a much smaller airgap, making it more difficult for the incident light to couple into the plasmonic mode. The S-polarized spectra shows very little change to the resonance structure up until 25 degrees, but at higher angles of incidence the amplitude of the resonance noticeably drops from 60% to 40% over the full range.

We further confirm the polarization insensitivity of the filter by plotting the S and P-polarized transmission of the ICP fabricated sample for a few different angles of incidence, as shown in Fig. 9. This figure shows that particularly for low angles of incidence there is very little change to the structure of the transmission spectra. At larger angles of incidence, the change in the P-polarized spectra is accounted for by the shifting of the substrate plasmonic resonance which can be reduced by shortening the period of the resonators thus shifting it out of the spectral range of interest. In the S-polarized spectra, there is a notable $\sim$20% decrease in the transmission of the filter accompanied by reduced spectral width of the resonance. We attribute this to weakened coupling between the incident plane wave and the cavity mode. This can potentially be solved by optimizing the geometry of the resonator and improving quality of the device via further fabrication efforts. Further, there is a shift in the resonant wavelength of the cavity at higher angles of incidence, most notably in the p-polarized spectrum where the plasmonic mode is involved. In such a case where there is not a significant contribution to the spectral response such as in the s-polarized spectra (also solved by reducing substrate index or array periodicity to move the plasmonic mode away from the region of interest), the change in the resonant wavelength is minimal compared to the linewidth of the resonance even at larger angles of incidence. This in turn will lead to only minimal changes in the optimal performance of the filter.

The current state of the art in terms of detecting technologies include, such as MCT, QWIP, and type II superlattices [21], [22], generally have broadband absorption spectra related to their bandgap. Integrating one of these filters onto such a detector allows for the development of multi-spectral pixels analogous to how modern color cameras work. This would allow for additional spectral properties to be used in identifying targets in search and track and other similar sensing applications.

IV. Conclusion

In conclusion, we have demonstrated both angle and polarization insensitive filtering in the mid-infrared spectral range using a dense array of dielectric micro-resonators. Our experimental results of the transmissive properties for both the resonator and substrate plasmonic mode of the structure have a strong correlation to our theoretical and simulated description of the system. By fine tuning the thickness and periodicity of the resonators, the resonator and plasmonic modes can be decoupled spectrally even at higher angles of incidence allowing for this geometry to create true angle and polarization-insensitive mid-infrared filters.

References

[1] I. Avrutsky, E. M. Smith, S. Vangala, R. Gibson, J. R. Hendrickson, and J. W. Cleary, "Angle- and polarization-independent mid-infrared narrowband optical filters using dense arrays of resonant cavities," *Opt. Exp.*, vol. 27, pp. 37481–37493, 2019.

[2] E. Popov, S. Enoch, G. Tayeb, M. Nevière, B. Gralak, and N. Bonod, "Enhanced transmission due to nonplasmon resonances in one- and two-dimensional gratings," *Appl. Opt.*, vol. 43, no. 5, pp. 999–1008, 2004.

[3] R. Merlin, "Pinholes meet Fabry-Perot: Perfect and imperfect transmission of waves through small apertures," *Phys. Rev. X*, vol. 2, no. 3, 2012, Art. no. 031015.

[4] V. Labeke, D. Gerard, B. Guizal, F. I. Baida, and L. Li, "An angle-independent frequency selective surface in the optical range," *Opt. Exp.*, vol. 14, no. 25, 2006, Art. no. 11945.

[5] V. Kanaev, M. R. Kutteruf, M. K. Yetzbacher, M. J. Deprenger, and K. M. Novak, "Imaging with multi-spectral mosaic-array cameras," *Appl. Opt.*, vol. 54, no. 31, pp. F149–F157, 2015.

[6] G. Perez et al., "Optical and structural characterization of single and multilayer germanium/silicon monoxide systems," *Thin Solid Films*, vol. 485, no. 1-2, pp. 274–283, 2005.

[7] Y. J. Jen and M. J. Lin, "Design and fabrication of a narrow bandpass filter with low dependence on angle of incidence," *Coatings*, vol. 8, no. 7, 2018, Art. no. 231.

[8] C. Sibilia, M. Scalora, M. Bertolotti, M. J. Blomer, and C. M. Bowden, "Electromagnetic properties of periodic and quasi-periodic one-dimensional, metallo-dielectric band gap structures," *J. Opt. A: Pure Appl. Opt.*, vol. 1, no. 4, pp. 490–494, 1999.

[9] Y. S. Lin and W. Chen, "A large –area, wide-incident-angle, and polarization-independent plasmonic color filter for glucose sensing," *Opt. Mater.*, vol. 75, pp. 739–743, 2018.

[10] C. M. Wang et al., "Angle-independent infrared filter assisted by localized surface plasmon polariton," *IEEE Photon. Technol. Lett.*, vol. 20, no. 13, pp. 1103–1105, Jul. 2008.

[11] T. W. Ebbesen, H. J. Lezec, H. F. Ghaemi, T. Thio, and P. A. Wolff, "Extraordinary optical transmission through sub-wavelength hole arrays," *Nature*, vol. 391, no. 6668, pp. 667–669, 1998.

[12] Q. Wang, Z. Zhu, H. Gu, and Q. Tan, "Angle-tolerant hybrid plasmonic blue filter with polarization-insensitivity and high transmission," *Opt. Commun.*, vol. 427, pp. 457–461, 2018.

[13] Q. Wang, Z. Zhu, H. Gu, M. Chen, and Q. Tan, "Multi-band transmission color filters for multi-color white LEDs based visible light communication," *Opt. Commun.*, vol. 403, pp. 330–334, 2017.

[14] L. Mashev and E. Popov, "Zero order anomaly of dielectric coated gratings," *Opt. Commun.*, vol. 55, no. 6, pp. 377–380, 1985.

[15] A. Avrutsky, G. A. Golubenko, V. A. Sychugov, and A. V. Tishchenko, "Light reflection from the surface of a corrugated waveguide," *Sov. Tech. Phys. Lett.*, vol. 11, pp. 401–402, 1985.

[16] A. Avrutsky and V. A. Sychugov, "Reflection of a beam of finite size from a corrugated waveguide," *J. Modern Opt.*, vol. 36, no. 11, pp. 1527–1539, 1989.

[17] R. Magnusson and S. S. Wang, "New principle for optical filters," *Appl. Phys. Lett.*, vol. 61, no. 9, pp. 1022–1024, 1992.

[18] K. Kintaka, T. Majima, J. Inoue, K. Hatanaka, J. Nishii, and S. Ura, "Cavity-resonator-integrated guided-mode resonance filter for aperture miniaturization," *Opt. Exp.*, vol. 20, no. 2, pp. 1444–1449, 2012.

[19] I. Avrutsky, "Resonant reflection by waveguide gratings with structured period," in *Proc. IEEE Res. Appl. Photon. Defense Conf.*, 2020, pp. 1–3.

[20] I. Avrutsky, M. Klein, S. Vangala, D. E. Walker, E. Smith, and J. R. Hendrickson, "Structured waveguide grating for controlled resonant reflection," in *Proc. IEEE Res. Appl. Photon. Defense Conf.*, 2023, pp. 1–2.

[21] C. Goldberg et al., "Comparison of HgCdTe and QWIP dual-band focal plane arrays," *Proc. SPIE*, vol. 4369, pp. 532–546, Oct. 2001.

[22] G. Ariyawansa, M. Grupen, J. M. Duran, J. E. Scheihing, T. R. Nelson, and M. T. Eismann, "Design and modeling of InAs/GaSb type II superlattice based dual-band infrared detectors," *J. Appl. Phys.*, vol. 111, no. 7, pp. 073107-1–073107-10, 2012.